

Electron momentum spectroscopy study of a conformationally versatile molecule: n-propanol

This article has been downloaded from IOPscience. Please scroll down to see the full text article.

2009 J. Phys. B: At. Mol. Opt. Phys. 42 165205

(<http://iopscience.iop.org/0953-4075/42/16/165205>)

View [the table of contents for this issue](#), or go to the [journal homepage](#) for more

Download details:

IP Address: 166.111.26.181

The article was downloaded on 06/05/2011 at 07:28

Please note that [terms and conditions apply](#).

Electron momentum spectroscopy study of a conformationally versatile molecule: n-propanol

Z H Luo, C G Ning, K Liu, Y R Huang and J K Deng

Department of Physics and Key Laboratory of Atomic and Molecular NanoSciences of MOE, Tsinghua University, Beijing 100084, People's Republic of China

E-mail: ningcg@tsinghua.edu.cn and djk-dmp@tsinghua.edu.cn


Received 24 October 2008, in final form 2 June 2009

Published 27 July 2009

Online at stacks.iop.org/JPhysB/42/165205

Abstract

As a continued study of structural versatile molecules, n-propanol ($\text{CH}_3\text{CH}_2\text{CH}_2\text{OH}$) has been investigated with our newly developed electron momentum spectrometer. n-propanol is a straight-chain molecule with one more carbon atom than ethanol. In order to verify the validity of the plane wave impulse approximation (PWIA), the measurements were conducted at impact energies of 1200 eV and 600 eV. The theoretical calculations of five known conformers: Tt, Tg, Gt, Gg, Gg' were performed by B3LYP/aug-cc-pVTZ and OVGf/6-311++G** methods with thermodynamic population analysis. This process can well simulate the measurements. Both measurements and theoretical simulations show that the one-electron binding energies and momentum distributions highly depend on the conformation. Depending on the conformation, a given orbital (e.g. MO11) may contribute to different bands in the (e, 2e) ionization spectrum. It was found that the momentum distributions can reflect the distortions and topological changes that molecular orbitals undergo due to the internal rotation of the hydroxyl and the distortion of the carbon chain.

 Supplementary data files are available in the online edition

(Some figures in this article are in colour only in the electronic version)

1. Introduction

n-propanol is a structural versatile molecule, which has five possible conformers at room temperature, Tt (*Trans-trans*), Tg (*Trans-gauche*), Gt (*Gauche-trans*), Gg (*Gauche-gauche*), Gg' (*Gauche-gauche'*), which are mainly distinguished by the dihedral CCCO and the dihedral HOCC, as shown in figure 1 and table 1. Using the infrared spectroscopy, the early works reported at least two stable conformers of n-propanol [1–3]. Through the research of the microwave spectrum, Imanov [4] and Abduranhmanova [5] confirmed the *trans* and *gauche* conformers, based on the C-C band center. Later, Abduranhmanova investigated a series of doublet transitions [6–9], which confirmed the assignment of Tt, Tg, Gt and Gg conformers. Dreizler and Scappini also investigated the ground state rotational spectrum of the Tt conformer of n-propanol [10]. Liu *et al* studied the O-H stretching vibrational

overtone and molecular conformations of n-propanol by the cavity ring down spectroscopy, and compared the results with the theoretical simulations of the five conformers Tt, Tg, Gt, Gg and Gg' which were optimized by the density function theory (DFT) at the level of B3LYP/6-311+G**, and the calculated O-H stretching frequencies and the stability were in good agreement with the experimental results [11]. n-Propanol also interests the chemistry of astrophysics, which may exist at observable quantities in the interstellar medium [12]. Maeda *et al* measured the millimeter- and sub-millimeter-wave spectra of the Gt conformer [13] for the purpose of helping astronomical identification. Duric *et al* measured the total electron impact ionization cross section of n-propanol molecules, in the incident electron energy range from threshold to 300 eV [14]. More recently Joarder *et al* investigated the molecular conformation and structural correlations of liquid D-1-propanol through neutron diffraction [15].

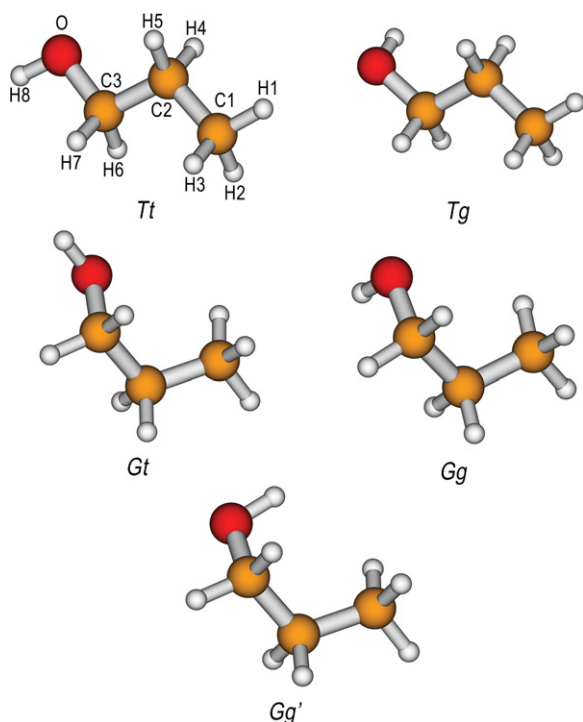


Figure 1. Geometry structures of the five conformers: Tt, Tg, Gt, Gg and Gg' of n-propanol.

Table 1. The main structural differences of the five conformers of n-propanol

Dihedral	Tt	Tg	Gt	Gg	Gg'
CCCO (degrees)	180	180	60	60	60
HOCC (degrees)	180	60	180	60	-60
Symmetry number	1	2	2	2	2

Besides the measurements of n-propanol, there were also many theoretical studies [16–20], which explored the molecular structures and relative energies of different conformers. Recently, Kahn and Bruice did the focal point conformational analysis of n-propanol by systematically improving the basis set and the level of electron correlations [21]. They studied the six conformers of n-propanol, Tt, Tg, Gt, Gg, Gg' and Gs. Since the Gs has a much higher relative focal-point energy (1.53 kcal mol⁻¹) [21], we mainly focus on the other five conformers in the present work.

Compared with the many investigations of the molecular structure of n-propanol, there are relatively scarce detailed studies of the electronic structures of this compound. The electronic wavefunction is very sensitive toward the conformational change, and the previous works [22–30] have demonstrated that the electron momentum spectroscopy is a powerful tool for investigating the conformational change. This work followed the guideline of previous works of Deleuse *et al* [24, 26, 27], which made use of the results of statistical thermodynamically calculations of conformer abundances along with Green's function calculations of ionization energies. The challenge for the case of n-propanol is the conformational diversity. In order to correctly unravel experiments employing electron momentum spectroscopy

onto conformationally versatile molecules, Deleuse *et al* indicated that it was essential to account for the influence of the conformation on the underlying valence ionization spectrum [31]. Depending on the conformation, a given orbital (e.g. MO 11 for n-propanol) may contribute to different bands in the (e, 2e) ionization spectrum.

2. Theory and experimental details

Electron momentum spectroscopy (EMS), a powerful tool for investigating the electronic structures [32–35], is based on a binary (e, 2e) experiment in which an incident electron with high enough energy E_0 induces ionization of a molecular target [36–39]. The scattered and ionized electrons are subsequently detected in coincidence at equal kinetic energies and equal polar angles, i.e. $E_1 \approx E_2$ and $\theta_1 \approx \theta_2 \approx 45^\circ$, hence at equal momenta $p_1 \approx p_2$. The initial momentum p of the knocked-out electron follows simple conservation rules:

$$p = \{(2p_1 \cos \theta_1 - p_0)^2 + [2p_1 \sin \theta_1 \sin(\phi/2)]^2\}^{1/2}, \quad (1)$$

where p_0 is the momentum of the incident electron. Triple differential cross section (TDCS) of (e, 2e) reaction contains rich information of the target structures and scattering dynamics. Within the Plane Wave Impulse Approximation (PWIA), the assumptions of the Born–Oppenheimer approximation (sudden or vertical), binary encounter and the independent one-particle model, the triple differential cross section can be written as

$$\sigma_{\text{EMS}} \propto \int d\Omega |\langle v_{\vec{p}} \Psi_f^{N-1} | \Psi_i^N \rangle|^2, \quad (2)$$

where $v_{\vec{p}}$ represents a plane wave function $e^{i\vec{p}\cdot\vec{r}}$. With the target Hartree–Fock approximation (THFA) or the target Kohn–Sham approximation (TKSA) [40, 41], upon the accounting for the dispersion of the ionization intensity over shake-up and shake-down satellites, equation (2) can be reduced as

$$\sigma_{\text{EMS}} \propto S_i^f \int d\Omega |\psi_i(p)|^2, \quad (3)$$

where $\psi_i(p)$ is the momentum space representation of a Hartree–Fock or Kohn–Sham orbital, and S_i^f is the associated spectroscopic factor, or called pole strength. S_i^f is related to the electron correlation, and meets the requirement of $\sum_i S_i^f = 1$.

As a structural versatile molecule, the relative abundance n_i of the five conformers of n-propanol correspondingly can be estimated with the Boltzmann statistics through the equation

$$n_i = \rho_i \exp(\Delta G/kT), \quad (4)$$

where k is the Boltzmann constant; ρ_i is the symmetry number of the conformer; ΔG is the best estimated Gibbs free energy relative to the most stable conformer Gt. With the focal point analysis reported by Kahn and Bruice [21], and the zero-point vibrational energy corrections, enthalpy and entropy corrections derived from the Boltzmann statistical thermodynamics that were computed at the B3LYP/aug-cc-pVTZ level, at standard temperature (298 K) and pressure (1 atm), using the RRHO (rigid-rotor harmonic oscillator)

approximation, the relative abundances of Tt, Tg, Gt, Gg and Gg' were 0.115, 0.214, 0.281, 0.195 and 0.195, respectively.

The theoretical simulations were all performed by using the density functional theory (DFT) along with the standard hybrid B3LYP functional [42] and aug-cc-pVTZ basis set in the Gaussian program [43]. The momentum distributions were generated by a newly developed program *NEMS* [44], which followed a general analytic formula for handling basis functions, regardless angular momentum quantum numbers.

The EMS spectrometer constructed in our laboratory took symmetric non-coplanar geometry, adopted a double toroidal energy analyzer and position sensitive detectors, in order to achieve the energy and angle multi-channel detections. The details were reported in previous works [45, 46]. To achieve a higher resolution, significant improvements were accomplished on the spectrometer [47]. A new electron gun equipped with an oxide cathode replaced the generic filament, since the much lower working temperature of the oxide cathode can improve the electron beam with a lower energy spread and divergence angle. A molybdenum aperture was introduced to constrain the electron beam in 0.35 mm diameter. The passing energy was set to 50 eV from 100 eV, in order to improve the energy resolution. With measures and optimization of electron optics adopting the Monte Carlo simulation, the angle resolutions, $\Delta\phi = \pm 0.84^\circ$ and $\Delta\theta = \pm 0.60^\circ$, were obtained by the standard calibration run for argon. The space charge effects make the energy resolution highly depend on the emitting current of cathode. In this experiment, the energy resolution was 0.68 eV (FWHM) through controlling the emitting current.

The n-propanol sample was a commercial product with a purity of 99%. No further purification was processed, and no impurity of the sample was observed in the binding energy spectra evidently.

3. Results and discussion

In this work, we mainly focus on the five stable conformers, Tt, Tg, Gt, Gg and Gg'. The geometrical structures of the five conformers of n-propanol have been optimized at the B3LYP/aug-cc-pVTZ level, with the starting inputs of experimental geometries.

3.1. Binding energy spectra

The observed momentum–energy (M–E) density map of n-propanol at the impact energy of 1200 eV plus binding energies is given in figure 2(a). The momentum–energy response function of the spectrometer was obtained by the standard calibration run for argon. Electron-binding energy spectra can be inferred from the density map for each azimuthal angle which defines the momentum of the electron prior to ionization. The overall characters of the M–E density map, although qualitative, could provide useful information for later orbital assignment of the binding energy spectra. The resolvable structures, labeled 1–9 as shown in figure 2(b), were obtained by integrating the (e, 2e) measurements over all azimuthal angles. In order to infer the experimental electron momentum distributions which characterizes each resolvable

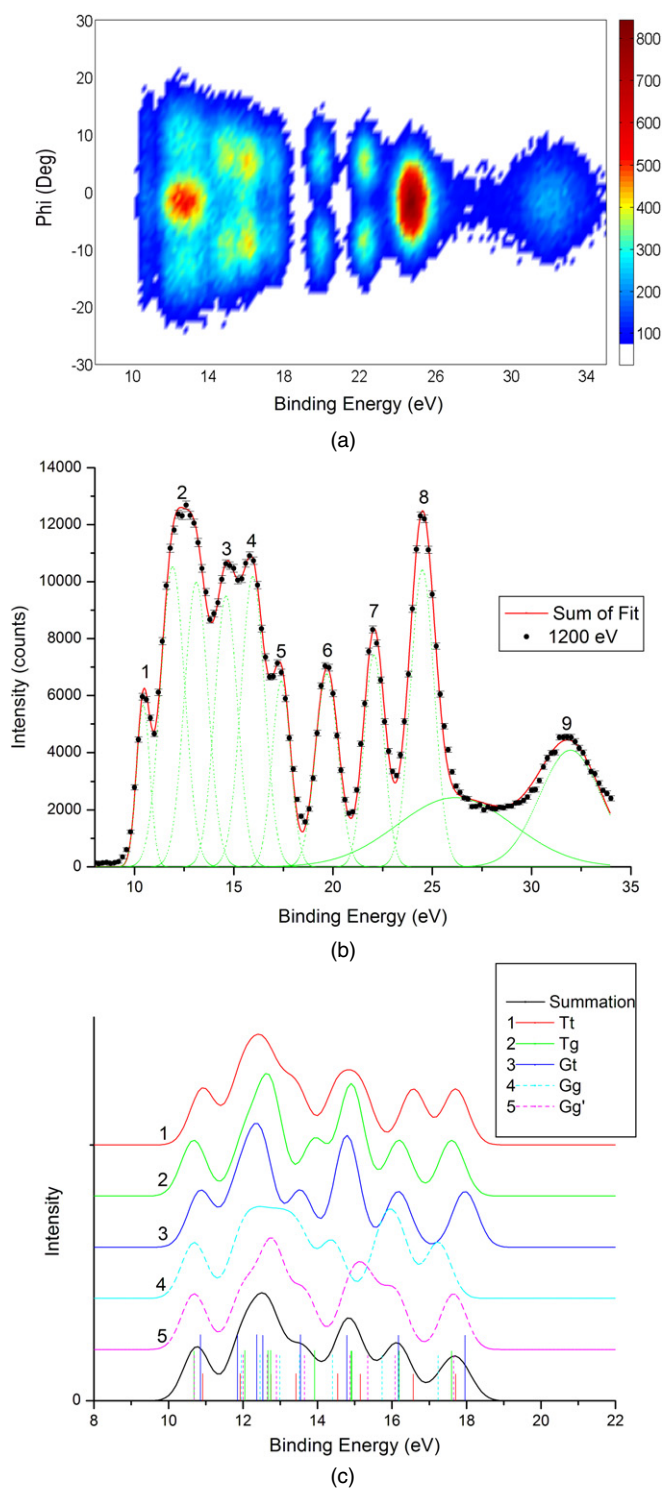


Figure 2. Binding energy spectra of n-propanol. (a) The valence momentum–energy density map of n-propanol measured at the impact energy of 1200 eV plus binding energies. (b) Experiment binding energy spectra summed over all ϕ angles at the impact energy of 1200 eV plus binding energies. The error bars represent one standard deviation. (c) The theoretical simulation of binding energy spectra of the five conformers Tt, Tg, Gt, Gg and Gg' calculated using the OVGf/6-311++G** method and their summation according to the Boltzmann statistics.

sets of orbital, the binding energy spectra at each azimuthal angle were fitted onto Gaussian functions. The centers and

Table 2. Ionization energies of n-propanol (in eV); EMS pole strengths are given in the brackets.

Peak	EMS ^a	PES (HeI) ^b	OVGF/6-311++G**					Orbital
			Tt	Tg	Gt	Gg	Gg'	
1	10.4	10.49	10.92 (0.92)	10.68 (0.91)	10.86 (0.92)	10.69 (0.91)	10.69 (0.91)	MO17
2	12.5	11.70	11.92 (0.92)	12.05 (0.92)	11.85 (0.92)	11.95 (0.92)	12.00 (0.92)	MO 16
		12.24	12.37 (0.92)	12.67 (0.92)	12.37 (0.92)	12.46 (0.92)	12.65 (0.92)	MO 15
		12.79	12.75 (0.91)	12.74 (0.92)	12.53 (0.91)	12.99 (0.91)	12.90 (0.92)	MO 14
3	14.6	(13.4)	13.42 (0.92)	13.92 (0.92)	13.54 (0.92)	13.52 (0.92)	13.65 (0.91)	MO 13
		14.52	14.54 (0.92)	14.90 (0.91)	14.79 (0.91)	14.40 (0.92)	14.87 (0.91)	MO 12
		(15.3)	15.15 (0.91)	14.92 (0.91)	14.79 (0.91)	–	–	MO 11
4	16.0	(15.3)	–	–	–	15.73 (0.91)	15.35 (0.91)	MO 11
		16.03	16.57 (0.91)	16.19 (0.91)	16.17 (0.91)	16.18 (0.91)	16.08 (0.91)	MO 10
5	17.4	17.23	17.71 (0.91)	17.60 (0.91)	17.96 (0.91)	17.24 (0.91)	17.65 (0.91)	MO 9
6	19.7 (0.77)							MO 8
7	22.1 (0.65)							MO 7
8	24.5 (0.45)							MO 6
9	32.0 (0.68)							MO 5

^a In our rescaling of experimental intensities, we assume that the pole strengths of the outer-valence orbitals are equal to 1.

^b See [48].

widths of those Gaussian functions were firstly determined from the high-resolution PES measurements [48], and then adjusted slightly for compensating the asymmetries in the shape of Franck–Condon envelopes. The peak related to the highest occupied molecular orbital (HOMO) was nicely resolved. The shape of peak 2 changes evidently at the different azimuthal angles. For a better description of its shape, two Gaussian functions were used to fit peak 2 which was related to four outer valence orbitals, i.e. MO16–13. Two broad Gaussian peaks in the inner valence region (more than 18 eV and less than 35 eV) were used to fit the congested satellite lines in this region, which were due to the breakup of orbital pictures [49].

In order to assign the observed binding energy spectra and precisely comprehend its structures, binding energy spectra were theoretically simulated by the OVGF/6-311++G** method [50–57] for each conformer (shown in figure 2(c)). The simulated spectra were obtained by convoluting the contributions from individual lines (given in table 2) by a Gaussian shape function with a full-width at half maximum (FWHM) of 0.8 eV which have considered the vibrational broadening and the energy resolution of the spectrometer. The solid black curve is the five conformers' summation incorporating their abundances according to the Boltzmann statistics. The heights of vertical lines under the curve represent the products of the pole strengths and the abundances. The simulated binding energy spectra have the approximately same profile with the measured ones: both have five main peaks in the outer valence region (<18 eV) and locate on approximately the same positions. Therefore, the theoretical simulation by the OVGF method, with the contributions from different conformers taking into account, is rather convincible.

The overlap of the congested electronic states induces the rich structures in the spectra partially washed out. Hence, part of information is unavoidably lost and results in a difficulty in separating each orbital. The extensive comparisons between theoretical simulations and experimental results have been executed. The binding energy of molecular orbital 11 (MO11)

is highly dependent on the conformation: it is 14.79 eV for Gt and 15.73 eV for Gg. This large difference makes Gt and Gg being grouped into two different peaks. As table 2 shows, MO11 (Gg) and MO11 (Gg') are grouped into peak 4, while MO11 (Tt), MO11 (Tg) and MO11 (Gt) are grouped into peak 3. This assignment is also supported by the observed momentum distributions. Therefore, for a conformationally versatile molecule, all possible stable conformations must be carefully taken into account for a correct interpretation of the experimental results. There are only eight blue vertical lines that can be seen in the spectra because the binding energies of MO12 and MO11 of Gt are essentially the same, i.e. 14.79 eV.

The further experiment at an impact energy of 600 eV was conducted in order to verify the validity of the plane wave impulse approximation (PWIA) for the reason that the PWIA was not valid for some valence orbitals [58–60].

3.2. Highest occupied molecular orbital (HOMO)

The highest occupied molecular orbital (HOMO) can be resolved from other orbitals. Its binding energy is 10.4 eV, related to peak 1 and labeled as MO17 (see table 2). The momentum distributions (MD) of HOMO measured at impact energies of 600 eV and 1200 eV are compared with theoretical calculations at the level of B3LYP/aug-cc-pVTZ, as shown in figure 3. The theoretical simulations of the orbital MDs have been convolved with the experimental momentum resolution at $E_0 = 1200$ eV using the Monte Carlo method [61]. Since the experimental momentum distributions are obtained in a relative scale, a proper normalization process must be employed. One of the normalization processes commonly used in the area of EMS was applied in the present study. It was that the experimental orbital MDs were normalized to the summation of the theoretical MDs in the outer region, i.e. peaks 1–5 in the binding energy spectrum (see figure 2(b)) were normalized to the corresponding summation of molecular orbitals 17–9 of n-propanol. The common normalization constant was used to normalize each outer valence orbital

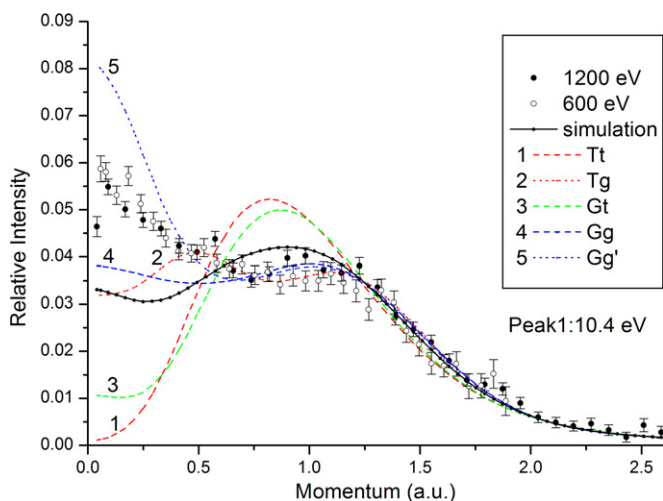


Figure 3. Convolved and spherically averaged momentum distribution of the HOMO of *n*-propanol at impact energies of 1200 eV and 600 eV. The error bars represent one standard deviation. The theoretical simulation is the sum of HOMO of Tt, Tg, Gt, Gg and Gg' according to the Boltzmann statistics.

and to calculate the pole strengths of the inner valence orbitals.

As shown in figure 3, the theoretical momentum distributions for each conformer display remarkable different characteristics. The HOMO of Tt is a typical *p*-type orbital, which has zero intensity at momentum origin $p = 0$ au, while Gg' is a *sp*-type which has a maximum intensity at $p = 0$ au and a hump at $p = 1.0$ au. The profiles of momentum distributions of conformers Tg and Gg have some median distributions of Tt and Gg', and Gt is more like Tt. The HOMOs for these conformers were further compared in a more familiar *r* space, as illustrated in figure 4. The oxygen lone pair O_{2p} and H_{1s} orbitals are the common components of HOMO for these conformers, which yield the hump at $p = 1.0$ au. The different stereo coordinates of atoms induce the different density maps and symmetry. Tt conformer has a mirror plane through the OCCO molecular backbone, which is also the node plane of its HOMO. Thus, its momentum distribution has zero intensity at $p = 0$ au. The HOMO of Gt conformer has a similar density map to that of Tt except the little distortion, which is due to the bend of the OCCO molecular backbone. Figure 4 also indicates that the Tg, Gg and Gg' all have a noticeable C-C bonding orbital, which yields a quite large intensity at $p = 0$ au.

For a convincing comparison between the experimental momentum distributions and theoretical calculations, the abundance of all possible conformers at the experimental conditions (see the black solid curve) have been taken into account in the simulation. In general, the simulation can describe the overall profile. However, there is a noticeable discrepancy between the simulation and experimental results in the low momentum region ($p < 0.5$ au). The simulation underestimates the experimental (e, 2e) cross section at the region of $p < 0.5$ au, which is the same phenomenon as we observed in the comparison between the theoretical calculation and the measured distribution of HOMO of ethanol [22]. One

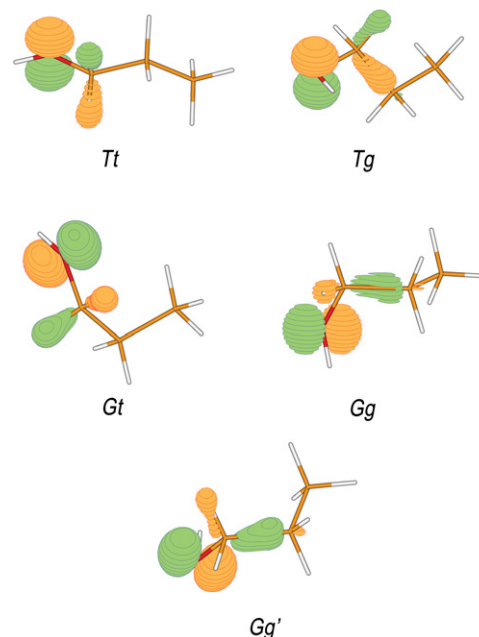


Figure 4. The density contour plots of HOMO of five conformers of *n*-propanol. The displayed molecular orbitals were drawn using Molden 4.3 with a density contour value of 0.12 [62].

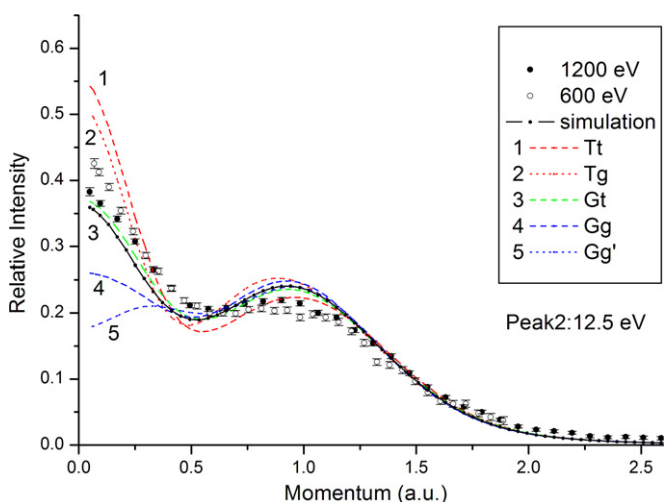


Figure 5. Convolved and spherically averaged momentum distributions of peak 2 of *n*-propanol at impact energies of 1200 eV and 600 eV which are related to MO16, 15, 14 and 13. The error bars represent one standard deviation. The theoretical simulation is the sum of MO16+15+14+13 of Tt, Tg, Gt, Gg and Gg' according to the Boltzmann statistics.

might explain this discrepancy using the distorted wave effects, which were recently observed in oxygen [58] and ethylene molecules [59]. However, the momentum distribution of HOMO at impact energies 600 eV does not show any noticeable difference from that of 1200 eV. Therefore, the plane wave impulse approximation (PWIA) is still valid. Although the HOMO of Gg' conformer is closer to the experimental distribution, it is not reasonable to increase the abundance of Gg' conformer. Because such an increase would lead stronger discrepancies between the theoretical and experimental momentum distributions of other outer-valence orbitals. A likely explanation is that some transitional

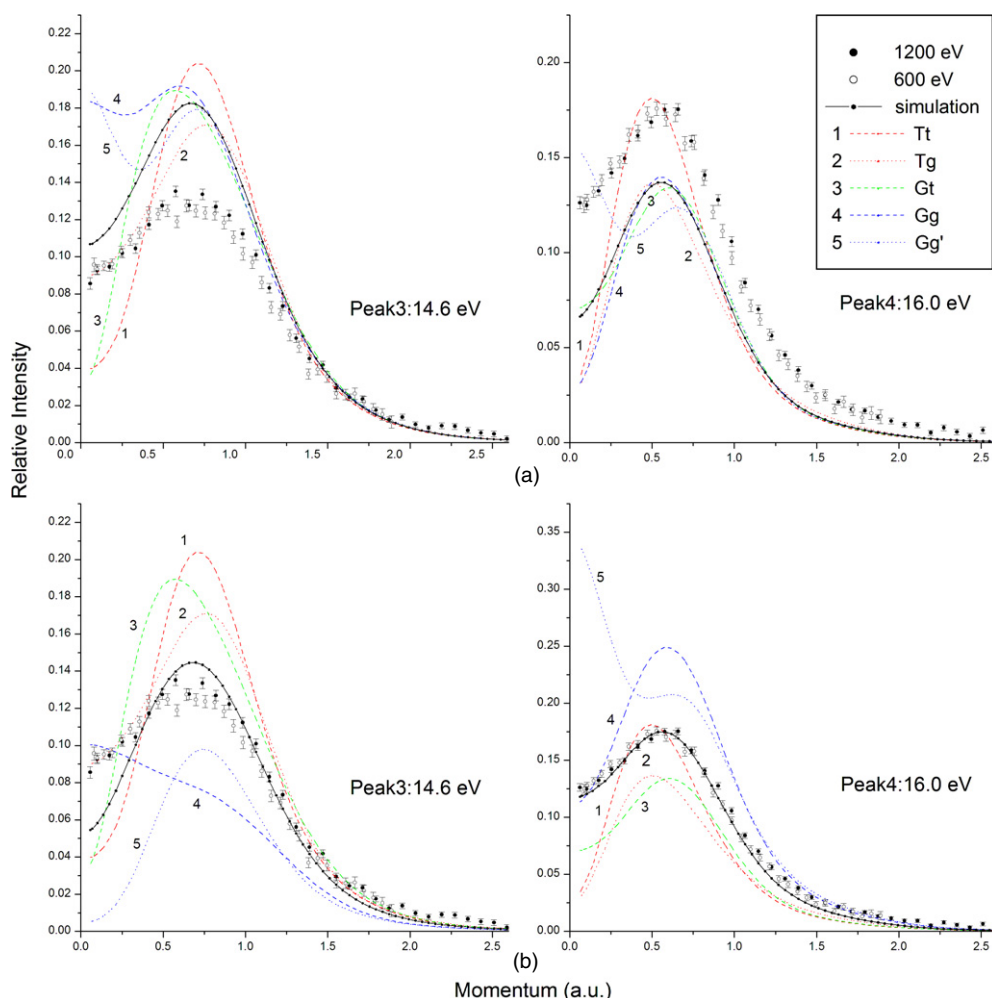


Figure 6. Convolved and spherically averaged momentum distributions of peaks 3 and 4 of n-propanol at impact energies of 1200 eV and 600 eV which are related to MO12, 11 and 10. The error bars represent one standard deviation. The theoretical simulations are the sums of MO12+11 and 11+10 of Tt, Tg, Gt, Gg and Gg' according to Boltzmann statistics, respectively. (a) MO12 and 11 of the five conformers are grouped into peak 3; MO10 belongs to peak 4. (b) Peak 3 includes MO12 of Tt, Tg, Gt, Gg and Gg' and MO11 of Tt, Tg and Gt; peak 4 includes MO11 of Gg and Gg' and MO10 of Tt, Tg, Gt, Gg and Gg'.

structures, which departures from equilibrium conformers can be noticeably populated for the rather shallow potential barriers. Another likely answer to this question is that the HOMO received considerable disturbance from peak 2. The experimental distribution is 0.025 greater than the theoretical simulation at the momentum origin, which is approximately 10% of experimental distribution of peak 2 at the same point. As shown in figure 2(b), the Gaussian function used to fit peak 2 penetrates quite deeply into the region of peak 1. Because of the asymmetry in the Franck–Condon envelope, the deconvolution technique using Gaussian functions is not the best choice in this case. An experiment with a higher energy resolution is expected to check this explanation.

3.3. Other outer valence orbitals

The other outer valence orbitals MO16–MO9 are congested in the region of the binding energy lower than 18 eV, where only four peaks can be resolved. Therefore, the experimental momentum distribution for each individual orbital cannot be

obtained due to the severe congestion. Instead, the summation of orbital clusters is investigated in this work.

Peak 2 located at 12.5 eV is related to MO16, 15, 14 and 13. The experimental data of impact energies at 1200 eV and 600 eV generally show a good agreement. The summation of momentum distributions of these orbitals of different conformers generally displays an *sp*-type in qualitative analysis. The five conformers have a gradually increased intensity in the low momentum region from Gg' to Tt, figure 5. The intensity ratios at the momentum origin of Gg', Gg, Gt, Tg and Tt are 1.8:2.6:3.7:5.0:5.4. The simulation can well reproduce the experimental distributions. Consequently, the relative abundances 0.115(Tt):0.214(Tg):0.281(Gt):0.195(Gg):0.195(Gg') obtained with thermodynamics are good predictions. The agreement between the simulation and experimental results also prevented the increase of the abundance Gg' to match the experimental distribution for HOMO. The slight differences between the 1200 eV data and the 600 eV data for peak 2 at ~ 0 au and 1.0 au may be caused by some distorted wave effects [58, 59] at the lower impact energy of 600 eV.

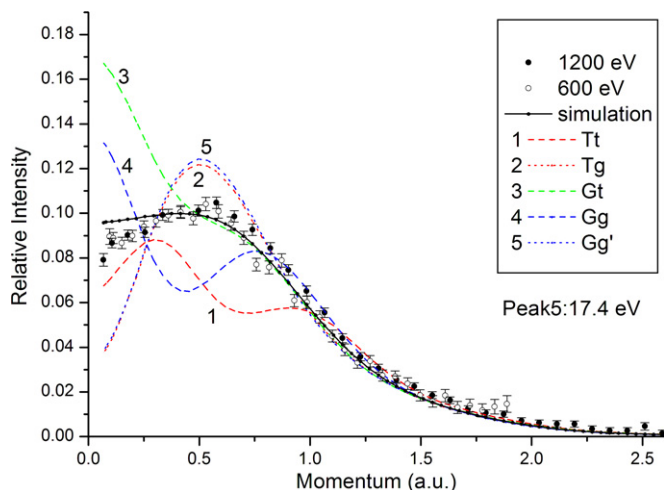


Figure 7. Convolved and spherically averaged momentum distributions of peak 5 of n-propanol at impact energies of 1200 eV and 600 eV which are related to MO9. The error bars represent one standard deviation. The theoretical simulation is the sum of MO9 of Tt, Tg, Gt, Gg and Gg' according to the Boltzmann statistics.

The advantage of EMS, which has the power of orbital ‘imaging’ and pole strength measuring, is demonstrated directly as the intensity distributions of peak 3 (14.6 eV) and peak 4 (16.0 eV) are analyzed. The binding energies of MO 12, 11 and 10 of the five conformers are within the range of 14.40–16.57 eV as indicated by the calculation of OVG/6-311++G** in table 2. Normally, we consider that MO 11 and 12 belong to peak 3, while MO 10 belongs to peak 4 for all five conformers. However, a huge discrepancy appears immediately, when the experimental distributions are compared with the theoretical simulations, figure 6(a). After carefully checking the binding energy of different conformers and their intensity distributions, we found that MO 11 of Gg and Gg' should be associated with peak 4 because their binding energies of 15.73 eV and 15.35 eV are closer to the center of peak 4 (16.0 eV) than that of peak 3 (14.6 eV). After this change was taken into the comparison, the agreements between the theoretical simulations and the experimental momentum distributions of peak 3 and peak 4 were improved greatly, figure 6(b). Consequently, MO12 of all five conformers and MO11 (Tt, Tg, Gt) are assigned to peak 3, while MO11 (Gg, Gg') and MO10 of all five conformers are related to peak 4. However, there is still an underestimation of the

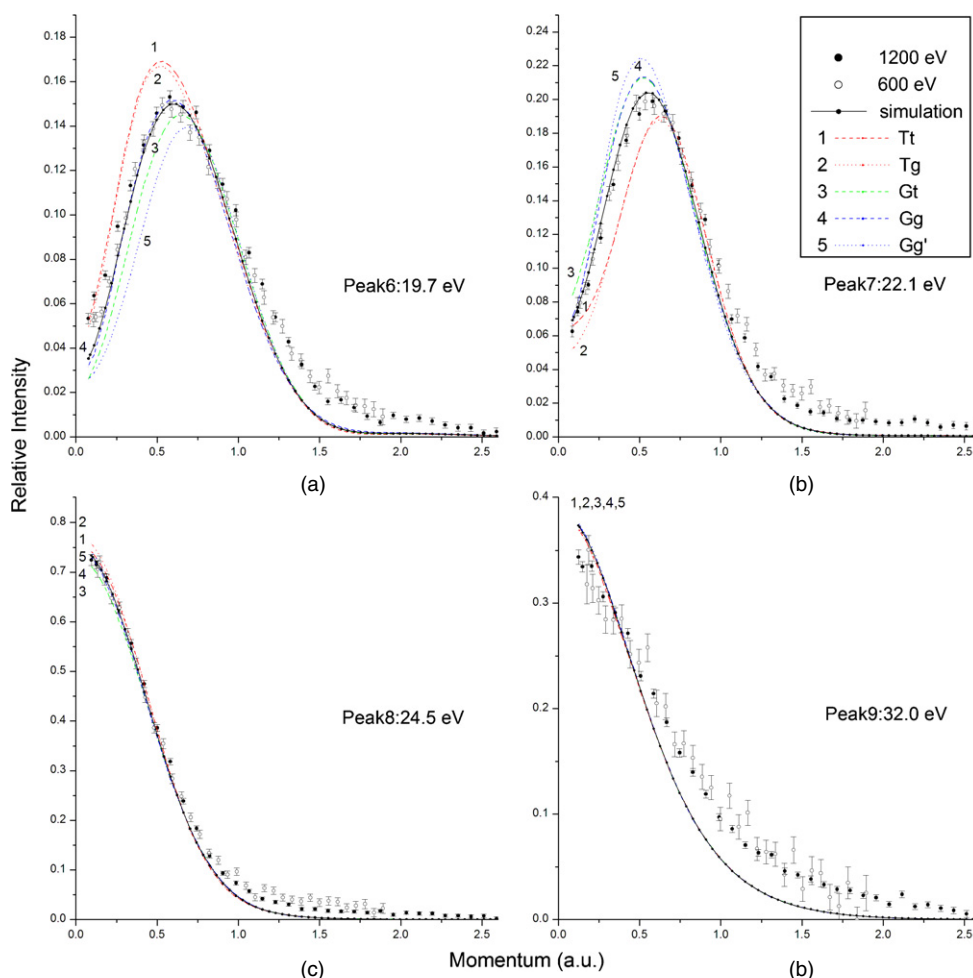


Figure 8. Convolved and spherically averaged momentum distributions of peaks 6, 7, 8 and 9 of n-propanol at impact energies of 1200 eV and 600 eV which are related to MO8, 7, 6 and 5, respectively. The error bars represent one standard deviation. The theoretical simulations are the sums of MO8–5 of Tt, Tg, Gt, Gg and Gg' according to the Boltzmann statistics, respectively.

experimental intensity by the theory at the low momentum region for peak 3. To explain this difference, we need to turn back to figures 2(b) and (c). In the binding energy spectrum figure 2(b), peak 3 is very close to peak 2. In figure 2(c), some orbitals which are related to peak 2 are very close to peak 3, such as MO13 of Tg. Hence, in such a multiple conformation situation, peak 3 receive considerable disturbance from peak 2. Since peak 2 is an *sp*-type with a high intensity near $p = 0$ au and peak 3 is a *p*-type with a zero intensity near $p = 0$ au, the measured intensity of peak 3 near the momentum origin is somewhat higher than the theoretical calculations.

MO9 of all five conformers are assigned to peak 5 (17.4 eV). The theoretical simulation can well reproduce the experimental momentum distributions, figure 7. Figure shows that the momentum distributions are strikingly different from one conformer to another. The orbital 9 of Gg conformer is a typical *sp*-type, while MO9 of Gg' and Tg are more like a *p*-type. The MO9 of Gt conformer displays an *s*-type distribution, which has a maximum intensity at the momentum origin. It then monotonically decreases as the momentum increases. The momentum distribution of MO9 of Tt conformer has two humps: one at 0.25 au and the other at 1.0 au. This indicates again that the momentum distributions for outer valence orbitals are sensitive toward the molecular conformational changes.

3.4. Inner valence orbitals

Figure 8 shows the momentum distributions in the inner valence region of 18–34 eV which is related to MO 8-5 and their satellite lines. Their pole strengths are noticeably less than 0.85, which implies the breakdown of orbital pictures in the inner valence region [35]. Peak 6 (19.7 eV) is related to MO8, and the momentum distributions of the five conformers are all *p*-type with a maximum at $p \sim 0.5$ au, figure 8(a), which are not sensitive toward the conformational change. Especially, the momentum, distributions of MO8 for Tt and Tg are nearly the same. The peak 7 (22.1 eV) is related to MO7, which is also *p*-type. As illustrated in figure 8(b), the profiles of MO7 of Tt and Tg are essentially identical, and so for Gt and Gg. This result shows that the dihedral HOCC change has little influence on their momentum distributions.

Peak 8 (24.5 eV) and peak 9 (32.0 eV) are related to MO6 and MO5, which are mainly composed of C_{2s} and O_{2s}, respectively. Their momentum distributions are totally insensitive to the different conformers. It should be noted that peak 9 includes both the main line of MO5 and many congested satellite lines from itself and other inner valence orbitals, and therefore the theoretical simulations using only the main line cannot well describe the experimental distribution.

4. Conclusions

The electronic structures and momentum-space intensity distributions of n-propanol were investigated with our newly developed electron momentum spectrometer with high resolutions. The measurements at the impact energies of 600 eV and 1200 eV plus the binding energies confirm the

validity of the plane wave impulse approximation (PWIA). The measurements are compared to Boltzmann-weighted simulations for the five known conformers (Tt, Tg, Gt, Gg and Gg') based on Kohn–Sham (B3LYP) orbital densities, as well as the outer valence Green's function calculations of one-electron ionization energies. The binding energy spectra were correctly assigned to the related molecular orbitals for the first time. It was found that both the binding energies and the momentum distributions in the outer valence region were very sensitive toward the conformational changes. Depending on the conformation, a given orbital (e.g. MO 11) may contribute to different bands in the (e, 2e) ionization spectrum. The consistency of theoretical simulations and observations indicates that the electron momentum spectroscopy could be used as a powerful probe of molecular conformations. In this study, a large discrepancy between the theoretical simulation and the experimental momentum distribution for the highest occupied molecular orbital (HOMO) was observed, the same phenomenon as we observed in the analysis of the HOMO of ethanol [22]. Since the momentum distribution is merely insensitive to the electron impact energy increasing from 600 eV to 1200 eV, a breakdown of the plane wave impulse approximation could not respond for the significant discrepancy. This discrepancy is probably caused by significant departures of the molecular structure from energy minima due to large-amplitude and thermal-induced motions. The disturbance from the neighboring orbitals is also a likely reason for the discrepancy because of the congestion of electronic states for n-propanol. Further experiments with a higher energy resolution and further simulations employing molecular dynamics are expected.

Acknowledgments

This work is supported by the National Natural Science Foundation of China under contract Nos 10704046 and 10575062, and Specialized Research Fund for the Doctoral Program of Higher Education under 20050003084.

References

- [1] Krueger P J and Mettee H D 1964 *Can. J. Chem.* **42** 347
- [2] Stuart A V and Sutherland G B B M 1956 *J. Chem. Phys.* **24** 559
- [3] Wilson E B 1972 *Chem. Soc. Rev.* **1** 293
- [4] Imanov L M, Abdurakhmanov A A and Ragimova R A 1968 *Opt. Spektrosk.* **25** 954
(English translation in 1968 *Opt. Spectrosc.* **25** 528)
- [5] Adburahmanov A A, Rahimova R A and Imanov L M 1970 *Phys. Lett. A* **32** 123
- [6] Abdurakhmanov A A, Burenin A V, Veliyulin E I, Imanova A L, Ragimova R A and Shapin S M 1978 *Izv. Akad. Nauk Azerb. SSR Ser. Fiz.-Tekh. Mat. Nauk* **1** 174
- [7] Abdurakhmanov A A, Veliyulin E I, Ragimova R A and Imanov L M 1981 *Zh. Strukt. Khim.* **22** 39
(English translation in 1981 *J. Struct. Chem.* **22** 28)
- [8] Abdurakhmanov A V and Ismailzade G I 1984 *Zh. Strukt. Khim.* **25** 177
(English translation in 1984 *J. Struct. Chem.* **25** 333)
- [9] Abdurakhmanov A A and Ismailzade G I 1987 *Zh. Strukt. Khim.* **28** 91
(English translation in 1987 *J. Struct. Chem.* **28** 238)

- [10] Dreizler H and Scappini F 1981 *Z. Naturforsch.* **36A** 1187
- [11] Liu Y L, Xu S C, Zhang L, Xu Y, Jiang B, Sha G H, Zhang C H and Xie J C 2000 *Chin. J. Chem. Phys.* **13** 513
- [12] Charnley S B, Kress M E, Tielens A G G M and Millar T J 1995 *Astrophys. J.* **448** 232
- [13] Maeda A, De Lucia F C, Herbst E, Pearson J C, Riccobono J, Trosell E and Bohn R K 2006 *Astrophys. J. Suppl. Ser.* **162** 428
- [14] Duric N, Cadez I and Kurepa M 1989 *Fizika* **21** 339
- [15] Sahoo A, Sarkar S, Krishna P S R, Bhagat V and Joarder R N 2008 *Pramana J. Phys.* **71** 133
- [16] Fukushima K and Zwolinski B J 1968 *J. Mol. Spectrosc.* **26** 368
- [17] Radom L, Lathan W A, Hehre W J and Pople J A 1973 *J. Am. Chem. Soc.* **95** 693
- [18] Siam K, Ewbank J D, Schafer L, van Alsenoy C and Allinger N L 1986 *J. Mol. Struct.* **32** 83
- [19] Schiel D and Richter W 1992 *J. Mol. Struct.* **266** 309
- [20] Gorbitz C H 1992 *J. Mol. Struct.* **94** 209
- [21] Kahn K and Bruice T C 2005 *Chem. Phys. Chem.* **6** 487
- [22] Ning C G, Luo Z H, Huang Y R, Hajgato B, Morini F, Liu K, Zhang S F, Deng J K and Deleuze M S 2008 *J. Phys. B: At. Mol. Opt. Phys.* **41** 175103
- [23] Ning C G, Huang Y R, Zhang S F, Deng J K, Liu K, Luo Z H and Wang F 2008 *J. Phys. Chem. A* **112** 11078
- [24] Huang Y R, Knippenberg S, Hajgato B, Francois J P, Deng J K and Deleuze M S 2007 *J. Phys. Chem. A* **111** 5879
- [25] Yang T C, Su G L, Ning C G, Deng J K, Wang F, Zhang S F, Ren X G and Huang Y R 2007 *J. Phys. Chem. A* **111** 4927
- [26] Knippenberg S, Huang Y R, Hajgato B, Francois J P, Deng J K and Deleuze M S 2007 *J. Chem. Phys.* **127** 174306
- [27] Deleuze M S, Pang W N, Salam A and Shang R C 2001 *J. Am. Chem. Soc.* **123** 4049
- [28] Wu F, Chen X J, Shan X, Tian S X, Li Z J and Xu K Z 2008 *J. Phys. Chem. A* **112** 4360
- [29] Zheng Y, Neville J J and Brion C E 1995 *Science* **270** 786
- [30] Falzon C T and Wang F 2005 *J. Chem. Phys.* **123** 214307
- [31] Deleuze M S and Knippenberg S 2006 *J. Chem. Phys.* **125** 104309
- [32] Takahashi M, Watanabe N, Khajuria Y, Udagawa Y and Eland J H D 2005 *Phys. Rev. Lett.* **94** 213202
- [33] Li Z J, Chen X J, Shan X, Xue X X, Liu T and Xu K Z 2008 *Chem. Phys. Lett.* **457** 45
- [34] Li Z J, Shan X, Yang X F, Chen L Q, Xu K Z and Chen X J 2008 *J. Phys. Chem. A* **112** 942
- [35] Knippenberg S, Nixon K L, Mackenzie-Ross H, Brunger M J, Wang F, Deleuze M S, Francois J P and Winkler D A 2005 *J. Phys. Chem. A* **109** 9324
- [36] Brion C E 1986 *Int. J. Quantum Chem.* **29** 1397
- [37] McCarthy I E and Weigold E 1991 *Rep. Prog. Phys.* **54** 789
- [38] Coplan M A, Moore J H and Doering J P 1994 *Rev. Mod. Phys.* **66** 985
- [39] Weigold E and McCarthy I E 1999 *Electron Momentum Spectroscopy* (New York: Kulwer/Plenum)
- [40] Duffy P, Chong D P, Casida M E and Salahub D R 1994 *Phys. Rev. A* **50** 4704
- [41] Zheng Y et al 1996 *Chem. Phys.* **212** 269
- [42] Lee C, Yang W and Parr R G 1988 *Phys. Rev. B* **37** 785
- [43] Frisch M J et al 1998 *Gaussian 98* (Pittsburgh, PA: Gaussian)
- [44] Ning C G, Hajgato B, Huang Y R, Zhang S F, Liu K, Luo Z H, Knippenberg S, Deng J K and Deleuze M S 2008 *Chem. Phys.* **343** 19
- [45] Ren X G, Ning C G, Deng J K, Zhang S F, Su G L, Huang F and Li G Q 2005 *Rev. Sci. Instrum.* **76** 063103
- [46] Ning C G, Deng J K, Su G L, Zhou H and Ren X G 2004 *Rev. Sci. Instrum.* **75** 3062
- [47] Ning C G, Zhang S F, Deng J K, Liu K, Huang Y R and Luo Z H 2008 *Chin. Phys. B* **17** 1729
- [48] Kimura K, Katsuwata S, Achiba Y, Yamazaki T and Iwata S 1981 *Handbook of HeI Photoelectron Spectra of Fundamental Organic Molecules* (New York: Halsted Press)
- [49] Cederbaum L S and Domcke W 1977 *Adv. Chem. Phys.* **36** 205
- [50] Ortiz J V 1988 *J. Chem. Phys.* **89** 6348
- [51] Cederbaum L S 1975 *J. Phys. B* **8** 290
- [52] von Niessen W, Schirmer J and Cederbaum L S 1984 *Comput. Phys. Rep.* **1** 57
- [53] Zakrzewski V G and von Niessen W 1993 *J. Comput. Chem.* **14** 13
- [54] Zakrzewski V G and Ortiz J V 1995 *Int. J. Quantum Chem.* **53** 583
- [55] Ortiz J V 1988 *Int. J. Quantum Chem. Symp.* **22** 431
- [56] Ortiz J V 1989 *Int. J. Quantum Chem. Symp.* **23** 321
- [57] Ortiz J V, Zakrzewski V G and Dolgounircheva O 1997 *Conceptual Perspectives in Quantum Chemistry* ed J-L Calais and E Kryachko (Dordrecht: Kluwer Academic) pp 465–518
- [58] Ning C G, Ren X G, Deng J K, Su G L, Zhang S F and Li G Q 2006 *Phys. Rev. A* **73** 022704
- [59] Ren X G, Ning C G, Deng J K, Zhang S F, Su G L, Huang F and Li G Q 2005 *Phys. Rev. Lett.* **94** 163201
- [60] Takahashi M, Saito T, Hiraka J and Udagawa Y 2003 *J. Phys. B: At. Mol. Opt. Phys.* **36** 2539
- [61] Duffy P, Casida M E, Brion C E and Chong D P 1992 *Chem. Phys.* **159** 347
- [62] Schaftenaar G and Noordik J H 2000 'Molden: a pre- and post-processing program for molecular and electronic structures *J. Comput.-Aided Mol. Design* **14** 123–34